Mode Projection Method for Target Mode Identification

Jeff Peck Marshall Space Flight Center EV31

A method for projecting flight configuration eigenvectors onto the vector space of the test configuration eigenvectors is proposed. The underlying concept of the proposed method is that any flight configuration eigenvectors that can be replicated by a linear combination of test configuration eigenvectors, is correlated, if the constituent test eigenvectors are themselves correlated. Therefore, the modal test target mode shapes should be those test modes that combine to form the important modes of the flight configurations. This approach also recognizes that it is the deformed shapes that dictate what sections of the structure are "highly strained" (in a relative since, within each mode shape), and that it is these highly strained sections that require an accurate stiffness representation to achieve an accurate model correlation.

Basic Equations

The critical feature that allows this process to work is that the test model and the flight models have a common set of physical degrees of freedom, or coordinates. This can be used to equate flight model mode shape(s) to a linear combination of the test model mode shapes. To illustrate, consider the test configuration model and the flight configuration model, represented in table 1 as different mass (M) and stiffness (K) matrices, and their associated eigenvalues, eigenvectors, and displacement vectors (λ, Φ, x).

Table 1. Test vs. Flight Models

Test Model	Flight Model
$M_t, K_t, \lambda_t, \Phi_t, x_t$	$M_f, K_f, \lambda_f, \Phi_f, x_f$

Because both the test and flight models contain common grids representing the same physical degrees of freedom, we may state that from a purely geometric standpoint, that an arbitrary displacement vector of the flight model (x_f) may be equivalently represented by a test model displacement vector (x_t).

$$x_t = x_f \tag{1}$$

Or, in terms of modal coordinates.

$$\Phi_t q_t = \Phi_f q_f \tag{2}$$

In general, we are interested in only selected flight modes. So, rewriting equation 2 to represent a single flight mode gives

$$\Phi_t q_{t,i} = \phi_{f,i} \tag{3}$$

Equation 3 represents a linear combination of the test modes shapes that reproduce flight mode *i*. We may then solve for the coefficients of the test modes ($q_{t,i}$) by pre-multiplying by the inverse of the test mode matrix (Φ_t^{-1})

$$q_{t,i} = \Phi_t^{-1}\phi_{f,i} \tag{4}$$

So theoretically, if the test and flight modes span the same vector space, and Φ_t^{-1} exists, we can solve for the linear combination of test modes that match a particular flight mode.

In practice, however, the test modes are not likely to (completely) span the flight mode vector space. This is due primarily to differences in boundary conditions (you can sum an infinite number of modes from a cantilever beam, but you will never match a free-free beam's 1st bending shape). Additionally, because we are generally limited to capturing only a small set of the test modes and degrees of freedom, the shapes we can replicate is limited even further. This means that a true inverse, Φ_t^{-1}, is not likely to exist, so to find q, we will have to settle for the pseudoinverse Φ_t^{+}. Then, instead of equation (4), let us write,

$$q_{t,i}^{+} = \Phi_t^{+}\phi_{f,i} \tag{5}$$

The pseudoinverse will basically provide an orthogonal projection of the flight mode onto the vector space spanned by the test modes, so there will be some degree of error between the flight mode ($\phi_{f,i}$) and its projection ($\Phi_t q_{t,i}^{+}$). This error can be represented as a vector as shown in equation 5.

$$\hat{e} = \phi_{f,i} - \Phi_t q_{t,i}^{+} \tag{6}$$

In 6, $\hat{e}$ represents the portion of $\phi_{f,i}$ outside of the vector space of Φ_t. The relationship between these vectors is illustrated in figure 1.

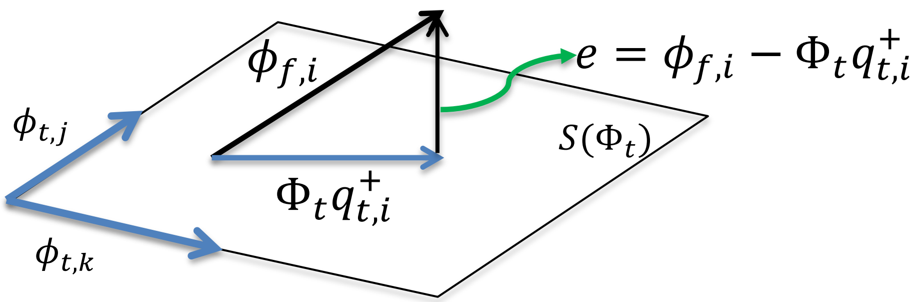

Figure 1. Relationship of vectors in equation 5

In figure 1, the plane labeled $S(\Phi_t)$represents the vector space spanned by Φ_t. The flight mode $\phi_{f,i}$ is shown as out of the plane of $S(\Phi_t)$, and the combination of test modes, $\Phi_t q_{t,i}^+$, is the orthogonal projection of $\phi_{f,i}$ onto $S(\Phi_t)$. The difference between the flight mode and it's orthogonal projection is the portion of the flight mode not spanned by Φ_t. This difference is represented by the error vector e.

The magnitude of e, $\|e\|$, is a usefull metric for measuring how closley the projected vector matches the original flight eigenvector. Equation 6 expresses $\|e\|$ as a precentage of the magnitude of the original flight vector, which we will call $\tilde{e}$. Low percentage values of $\tilde{e}$ are indicitave of a good match between the flight vector and the projected vector.

$$\tilde{e} = \left(\frac{\|e\|}{\|\phi_{f,i}\|}\right) * 100 \tag{7}$$

So our procedure is to calculate the unknown $q_{t,i}^+$ from 5, then calculate how closely the projection matches the original flight mode with equations 6 and 7.

Several methods could be used to calculate $q_{t,i}^+$. If the mass matrix of the test configuration model is available, then equation 3 could be multiplied by $\Phi_t^T M_t$, which is essentially the pseudoinverse of Φ_t (i.e. Φ_t^+) since our mode shapes are mass normalized such that $\Phi_t^T M_t \Phi_t = I$. The problem with this approach for the SLS IMT configuration, is that the mass matrix is dominated by the ML. Thus, once we perform the Guyan reduction of the mass matrix down to the vehicle only DOF's needed for compatability with equation 3, the orthogonality with the paritioned IMT modes is poor.

The most robust method found thus far for calculating the pseudoinverse of Φ_t is using singular value decomposition (SVD). SVD allows any matrix to be written as a product of three matrices as shown in equation 8.

$$\Phi_t = U\sigma V^T \tag{8}$$

Where U and V are orthogonal matrices containing the left and right singular vectors, and σ is a diagonal matrix of the singular values. Having this decomposition allows one to write the pseudoinverse as

$$\Phi_t^+ = V\sigma^{-1}U^T \tag{9}$$

Here, σ^{-1} is a matrix with the reciprocals of the non-zero singular values on the main diagonal and zeros everywhere else. For numerical implementations, only elements larger than some small tolerance value are taken to be non-zero, with all other values set to zero.

For the purpose of this study, the ability to select a range of zero tolerances is an advantage of using the SVD method to compute the pseudoinverse. By varying the zero tolerance, the user has control over number of singular values retained in the pseudoinverse, and thus has some control over the degree of singularity of the test modal matrix (Φ_t). It has been observed that it is advantageous to select a range of thresholds, and choose the best solution from the resulting set of $q_{t,i}^+$vectors. It seems that different flight vectors are better represented using different numbers of singular value/vector sets.

Numerical Implementation

When implementing the concepts of the previous section in a numerical setting, there are several issues that need to be addressed. First, the set of DOF to be equated between test and flight must be chosen. Second, a method for selecting the zero threshold for the singular values is needed. Third, since the desired outcome of the overall assessment is to have a small set of test target modes, we need a strategy for identifying and removing the unimportant modes from a projection. These issues are discussed in the following paragraphs and an outline of the resulting algorithm is presented in figure 2.

Choosing the set of physical DOF's to equate between the test and flight modal matrices has a large impact on the projection results. Because the flight modes of interest for the SLS are primary modes (i.e. 1st & 2nd bending, 1st torsion, ...), choosing DOF's that are highly active in shell modes or other localized modes is not likely to generate the desired results. For this reason, the model center line grids

(CLGs) were chosen as the DOF's to equate. The CLGs perform a good job of capturing the gross motion of the structure under the fundamental modes, and are also available in the ASET for both the delivered loads and GNC flex models. This last point is very important, because the CLG's are in the delivered loads and GNC models, the mode shapes from these models may be used directly (as opposed to performing a special model integration from either the bulk data models or the element delivered reduced substructures). The ability to directly use the mode shapes from the delivered Loads and FLEX models is important for better traceability to the loads and GNC analyses.

As was hinted at in the basic equation discussion, numerical implementations of the pseudoinverse require that a threshold be specified for determining which singular values are considered zero. This, along with the task of finding the minimum number of vectors needed to reasonably represent the flight mode, is addressed by searching a large number of solutions, and choosing the one producing the best results. The algorithm for calculating this "optimal" mode projection is essentially four nested loops; the flight mode loop, the singular value loop, the basis reduction loop and the sensitivity loop. Refer to figure 1, and the following paragraphs for a description of these loops

The flight mode loop is the top most of the four loops. It simply drives the other three loops over each flight mode provided to the program.

The singular value loop sets the zero tolerance used in calculating the pseudoinverse. It does this by performing an initial singular value decomposition, and then setting he zero tolerance equal to the first singular value. Control is then passed to the next lower loop. Once control is returned, it calculates the best solution stored for the current zero tolerance. The zero tolerance is then reset to the next singular value and the loop repeats until all singular values have been used.

The basis reduction loop takes the zero tolerance set in the singular value loop and calculates the pseudoinverse. It then solves for the generalized coordinates, and saves these results, along with some accuracy metrics. The test mode shape having the least influence on the solution accuracy is then removed, and a new pseudoinverse/projection is performed (using the same zero tolerance). This process is repeated until only a single test eigenvector remains and a solution for this one vector modal matrix is calculated. Control is then returned to the singular value loop.

The test mode shape with the least influence on the solution is found in the sensitivity loop. This loop assesses each generalized coordinate (GC) in turn, and calculates a sensitivity vector indicating the importance of each GC. This is done by sequentially setting each GC to zero, and then calculating the error vector magnitude (EVM) in equation 6 (not normalized with flight vector magnitude as in equation 7). Note that as each GC is set to zero, the previous GC that was set to zero is returned to its original value when entering this loop. This sensitivity vector is passed back to the basis reduction loop, for use in selecting the test mode shape to remove.

A flow chart of this procedure is presented in figure 2. Overall, this algorithm takes something of a brute force approach, as it examines a lot of different solutions. It is not quite a comprehensive examination of the solution space though, since within the basis reduction loop, the zero tolerance is fixed based on the full Φ_t decomposition, and as each (low importance) test mode is removed from consideration, the zero tolerance does not change to reflect the new singular values. This means the algorithm probably does not examine the zero cutoff for each singular value in the decomposition as the test modes are eliminated, and this could cause some solutions to be missed. Although the solutions produced by the current algorithm look quite good, future updates will attempt to address this potential sort coming.

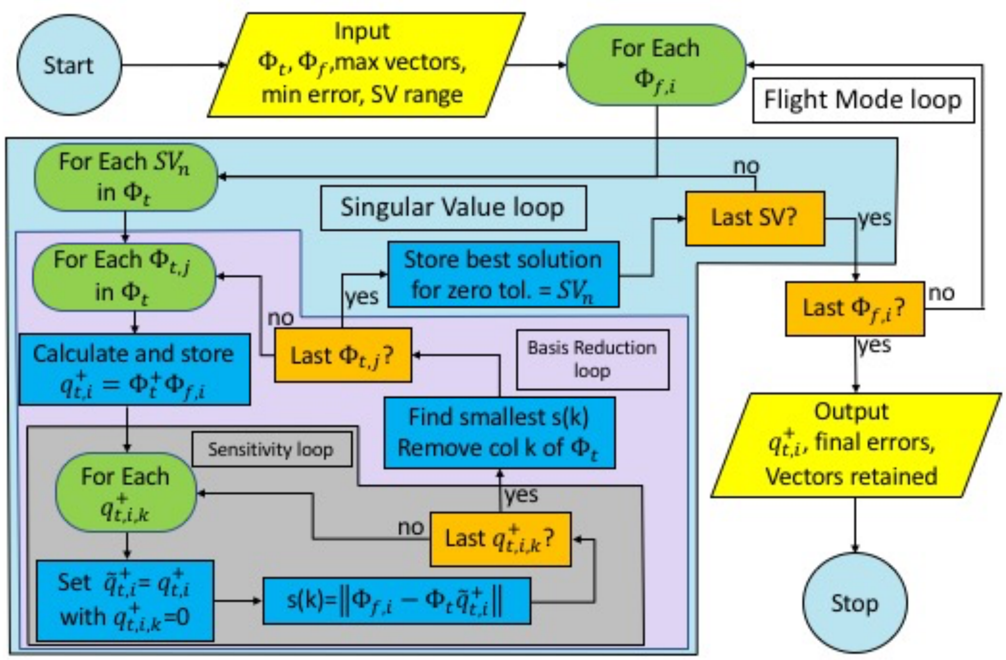

Figure 2. Numerical Algorithm Flow Chart

Analysis

A series of modal projections have been performed for the SLS IMT configuration. The most recent used the DTaMSS R3B model (for the IMT modes, this version included the "r3v5" version of the ML model) and the VAC1R loads models (for the flight modes). At the time of this analysis, the driving mode shapes from the VAC1R loads analyses were not yet available, so in leu of these, the first three bending mode pairs were projected onto the IMT modes. Also, given that the general configuration of the IMT most closely resembles the boost phase of flight, it was deemed appropriate to only project the boost phase modes from the Loads models for target mode identification.

Two different projections studies were created with the VAC1R/DTaMSS R3 models. One used the DTaMSS R3 target mode set of 30 IMT modes as the test mode basis. This set was selected using traditional approaches such as kinetic energy, modal effective mass, and engineering judgment. Another target mode set that included all "available" IMT modes up to 6.5 Hz was also used as the test mode basis. This latter set, which are referred to as the "full" set, excludes slosh modes, and other modes having the majority of their KE in the generalized coordinates of the DTaMSS model. Both projection analyses used only the translational degrees of freedom (DOF) of the centerline grids as the DOF to equate (see equation 1). Comparing the results from the projections on the two separate bases has a couple of purposes. First, projecting onto the 30 IMT target mode set will show how well this set maps to the flight modes, and should indicate which flight modes are captured, and possibly which of the 30 modes do not project to any flight modes. Second, the projection onto the full set may indicate some modes, not in the current target mode set, that, if included as target modes, may improve the representation of the flight modes

For each of the projection studies, three convergence criterion were established to aid in judging which modes were captured by the projection. The three convergence criterion are as follows; the number of IMT modes retained below 11 (indicated by "k"), error vector magnitude below 10% (equation 7, indicated by "e"), and all generalized coordinates below 4.0 (absolute value, indicated by "q"). To aid in visualization, a color code was established to compliment these criterion when results are presented in tabular format (see tables 2 and 3). The color code is as follows. When all three convergence criterion are met, the block is colored green. If the number of IMT modes retained exceeds 5, but the error and GC criterion are met, the block is colored yellow. If either the error or the GC criterion fail, the block is colored red. These thresholds are shown in tabular format in table 1.

Table 1. Convergence Criterion

Criterion	Label	Threshold	Green if	Yellow if	Red if
# of test modes in solution	k	<= 5	True	False	Any number
Error vector magnitude	e	<= 10%	True	True	either e or q are False
Max absolute value of and GC	q	<= 4.0	True	True	

The values for the thresholds are somewhat subjective and based primarily on experience from earlier projection analyses. The best evidence that any particular projection result accurately represents a flight mode is to replicate the linear combination of the test modes in NASTRAN and compare the deformed shape of the model from the linear combination to the deformed shape of the flight mode. While performing past combination to flight mode comparisons, the general observation has been that solutions meeting all three of the criterion in table 1 tend to show good agreement between the combination deformed shape and the flight mode deformed shape.

Results

An overview of the results of the projection onto the DTaMSS R3 target mode set is shown in table 2. The table lists the flight modes as the column headings and the flight times (and core stage fill levels) as the row headings. The color of each square indicates the level of convergence of the mode based on the three convergence criterion of table 1.

Table 2. Projection Results using IMT Target Mode Set

	1st XY	1st XZ	2nd XY	2nd XZ	3rd XY	3rd XZ
T0_F100	k 3 e 9.92 q 2.9	k 2 e 9.76 q 1.4	k 3 e 9.99 q 0.5	k 3 e 9.57 q 0.4	k 5 e 9.78 q 0.6	k 7 e 9.93 q 1.0
T10_F100	k 3 e 9.10 q 2.9	k 2 e 8.44 q 1.0	k 3 e 9.76 q 0.5	k 3 e 9.55 q 0.4	k 4 e 9.23 q 0.7	k 8 e 8.57 q 1.3
T20_F100	k 4 e 9.83 q 1.7	k 2 e 9.91 q 0.9	k 3 e 9.70 q 0.5	k 3 e 9.73 q 0.5	k 3 e 9.63 q 0.6	k 7 e 9.83 q 2.1
T30_F95	k 3 e 8.11 q 1.8	k 2 e 9.11 q 1.1	k 3 e 9.72 q 0.6	k 4 e 7.27 q 0.5	k 3 e 9.49 q 0.7	k 10 e 9.88 q 1.2
T40_F95	k 3 e 6.95 q 1.9	k 2 e 8.70 q 1.1	k 3 e 9.50 q 0.6	k 3 e 9.93 q 0.7	k 4 e 8.74 q 0.7	k 8 e 9.70 q 1.4
T50_F90	k 3 e 8.83 q 0.7	k 2 e 8.59 q 1.1	k 2 e 9.85 q 0.7	k 2 e 9.39 q 1.6	k 4 e 8.93 q 0.7	k 10 e 9.94 q 1.5
T60_F90	k 3 e 9.91 q 0.8	k 2 e 8.65 q 1.1	k 3 e 7.34 q 0.6	k 2 e 9.26 q 1.5	k 4 e 9.04 q 0.7	k 9 e 9.93 q 1.6
T70_F85	k 3 e 9.55 q 0.9	k 2 e 8.67 q 1.1	k 2 e 9.04 q 0.7	k 3 e 8.40 q 0.7	k 4 e 9.76 q 0.6	k 16 e 9.92 q 2.1
T80_F85	k 3 e 9.88 q 0.9	k 2 e 8.84 q 1.1	k 2 e 8.86 q 0.8	k 2 e 8.98 q 1.4	k 5 e 8.88 q 0.8	k 14 e 9.97 q 1.9
T90_F85	k 3 e 9.77 q 0.8	k 2 e 9.06 q 1.0	k 2 e 9.59 q 0.7	k 2 e 9.28 q 1.3	k 5 e 8.49 q 0.9	k 15 e 9.86 q 2.0
T100_F80	k 2 e 8.21 q 3.7	k 2 e 9.48 q 1.0	k 6 e 10.00 q 0.9	k 2 e 9.85 q 1.2	k 5 e 9.15 q 0.9	k 28 e 10.00 q 92.5
T110_F80	k 3 e 7.03 q 0.8	k 2 e 9.89 q 1.0	k 2 e 8.85 q 0.9	k 2 e 8.85 q 1.2	k 6 e 9.23 q 0.9	k 28 e 9.98 q 3.7
T120_F75	k 2 e 7.87 q 3.9	k 2 e 6.60 q 1.2	k 2 e 8.65 q 0.9	k 2 e 9.12 q 1.2	k 8 e 9.73 q 2.1	k 25 e 9.98 q 3.4

Looking at these results, it appears that the first 2 bending mode pairs are well represented by the 30 IMT target modes, with most only requiring 2 or 3 IMT modes to meet the error and generalized coordinate criterion. The third XY bending mode also seems well captured with the possible exception of the last couple of flight times. But the 3rd XZ bending mode is obviously harder to replicate, with the T100_f80 solution displaying very high q values.

Table 3. Projection Results using Full Mode Set

	1st XY	1st XZ	2nd XY	2nd XZ	3rd XY	3rd XZ
T0_F100	k 3 e 9.92 q 2.9	k 2 e 9.76 q 1.4	k 3 e 9.99 q 0.5	k 3 e 9.57 q 0.4	k 4 e 9.77 q 1.6	k 7 e 9.07 q 1.3
T10_F100	k 3 e 8.93 q 3.0	k 2 e 8.44 q 1.0	k 3 e 9.76 q 0.5	k 3 e 9.55 q 0.4	k 4 e 9.23 q 0.7	k 7 e 9.12 q 1.3
T20_F100	k 4 e 9.83 q 1.7	k 2 e 9.91 q 0.9	k 3 e 9.70 q 0.5	k 3 e 9.73 q 0.5	k 3 e 9.63 q 0.6	k 8 e 8.79 q 1.3
T30_F95	k 3 e 7.66 q 3.5	k 2 e 9.11 q 1.1	k 3 e 9.72 q 0.6	k 3 e 8.94 q 0.5	k 3 e 9.49 q 0.7	k 9 e 9.80 q 1.8
T40_F95	k 2 e 9.31 q 3.0	k 2 e 8.70 q 1.1	k 3 e 9.50 q 0.6	k 3 e 9.93 q 0.7	k 4 e 8.74 q 0.7	k 8 e 9.65 q 2.0
T50_F90	k 2 e 9.89 q 3.4	k 2 e 8.59 q 1.1	k 2 e 9.85 q 0.7	k 2 e 9.39 q 1.6	k 4 e 8.93 q 0.7	k 10 e 9.78 q 1.6
T60_F90	k 2 e 8.26 q 3.2	k 2 e 8.65 q 1.1	k 3 e 7.34 q 0.6	k 2 e 9.26 q 1.5	k 4 e 9.04 q 0.7	k 10 e 9.87 q 1.9
T70_F85	k 2 e 9.06 q 3.6	k 2 e 8.67 q 1.1	k 2 e 9.04 q 0.7	k 2 e 8.88 q 1.4	k 4 e 9.76 q 0.6	k 13 e 9.78 q 1.9
T80_F85	k 2 e 9.62 q 3.6	k 2 e 8.84 q 1.1	k 2 e 8.86 q 0.8	k 2 e 8.98 q 1.4	k 5 e 8.88 q 0.8	k 13 e 9.87 q 1.9
T90_F85	k 2 e 8.53 q 3.6	k 2 e 9.06 q 1.0	k 2 e 9.59 q 0.7	k 2 e 9.28 q 1.3	k 5 e 8.49 q 0.9	k 17 e 9.99 q 3.2
T100_F80	k 2 e 8.21 q 3.7	k 2 e 9.48 q 1.0	k 6 e 10.00 q 0.9	k 3 e 8.09 q 0.7	k 5 e 9.15 q 0.9	k 32 e 10.01 q 19.9
T110_F80	k 2 e 8.12 q 3.7	k 2 e 9.89 q 1.0	k 2 e 8.85 q 0.9	k 2 e 8.85 q 1.2	k 6 e 8.43 q 1.8	k 32 e 9.91 q 2.5
T120_F75	k 2 e 7.87 q 3.9	k 2 e 6.60 q 1.2	k 2 e 8.65 q 0.9	k 2 e 9.12 q 1.2	k 9 e 8.97 q 1.1	k 31 e 9.93 q 2.7

Table 3 shows the results of the projection onto full set. For the most part, these solutions are identical to the ones from the 30 mode target set, and those that are different don't indicate a substantially better solution. So including the extra 20 modes into the projection analysis does not seem to improve the answer, and therefore no expansion of the 30 target mode set is indicated. The following discussions will focus on the solutions from Table 2.

The "best" matches for each flight mode of Table 2 are highlighted with heavy boarders. In this situation, "best" is measured by selecting the solution(s) with the fewest retained modes and then the lowest percent error. These solutions were examined closer to better understand how well they captured the intended shape.

Closer examination of the highlighted solutions first compared the deformed shapes of the projection solutions to the deformed shapes from the VAC1R flight models.

These comparisons were done with just the centerline grid deflections in order to better visualize how the projection process saw the shapes, and to help identify what part of the projection the error was coming from. Second, a NASTRAN DMAP program was used to read in the solution generated by the MATLAB code, and replicate the indicated linear combination with the full G set sized IMT mode shapes. The resulting deformed shape was this passed through the NASTRAN data recovery process to generate full model deformations and strain energy fringe plots. Plotting the NASTRAN results in PATRAN allows a qualitative assessment of how well the solution, arrived at from the centerline grid deformations, reproduces the flight modes of the full model.

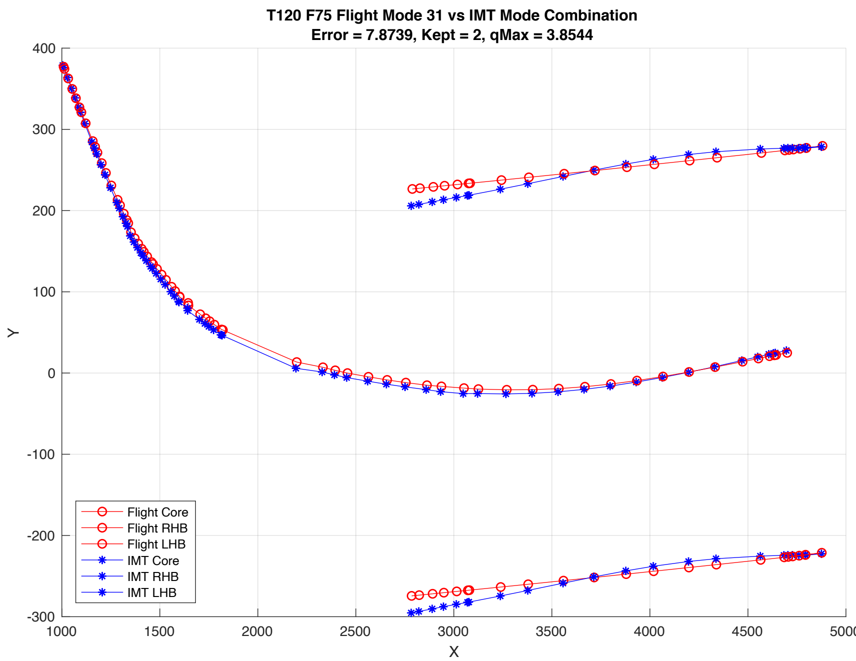

Figure 3. IMT vs. Flight Centerline deformations of 1st XY bending mode

Figures 3 and 4 show the centerline and full model plots for the first XY bending mode (T120_F75). The core vehicle portion of this mode is well represented by the linear combination of 2 IMT modes although the booster sections show more of a rigid body rotation in the flight mode while the IMT deformation exhibits more booster bending. This is not completely surprising since the IMT boundary conditions for the core vehicle are much more similar to flight than are the booster boundary conditions.

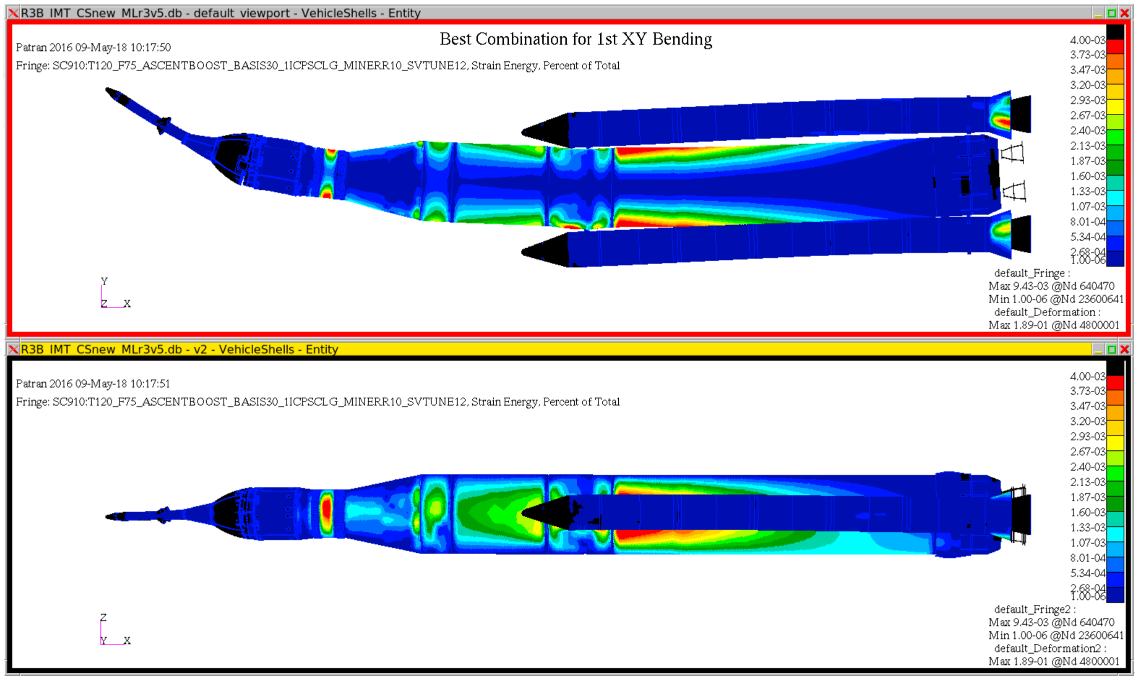

Figure 4. 1st XY best combination of IMT modes on full model (ML not pictured).

Figures 5 and 6 show plots for the first XZ bending mode. This mode also shows close agreement between the flight and projection shapes for the majority of the core portion of the vehicle. For the boosters, we see that the deflection error is located mostly near the aft where the IMT model (and thus the projection shape) is constrained.

Looking at Figure 5, in the aft end of the core vehicle there is notable deviation from the flight deflections. This appears to be due to resistance to deformation in the Z direction through the aft booster interfaces. When this is compared to Figure 3, where the aft core centerline deflections match quite well, it is noticed that the booster aft centerline deflections also show good agreement between flight and IMT. This trend appears in the remainder of the centerline deflection plots as well. When the IMT aft booster centerline deflections match flight, the IMT aft core also matches flight, and when the IMT aft boosters deviate, the aft core deviates. This happens for both XY and XZ modes and so is not dependent on which plane the mode is in.

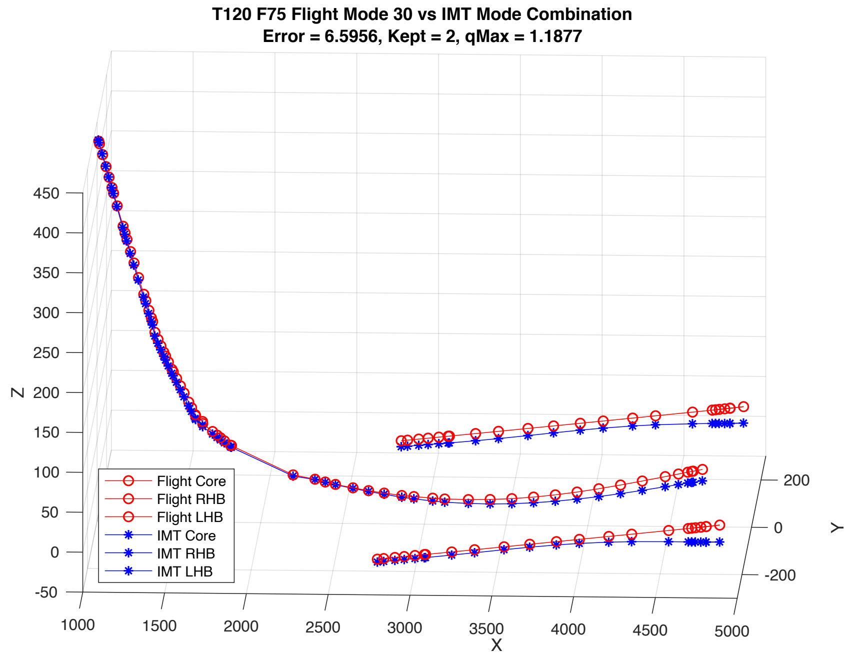

Figure 5. IMT vs. Flight Centerline deformations of 1st XZ bending mode

For the most part, the full model deformations and strain energy fringe plots show the desired shapes and distributions. It does appear that in all of these plots the vast majority of the strain energy is in the core vehicle while relatively little strain energy is in the boosters. The booster aft skirt does seem to be the exception to this rule.

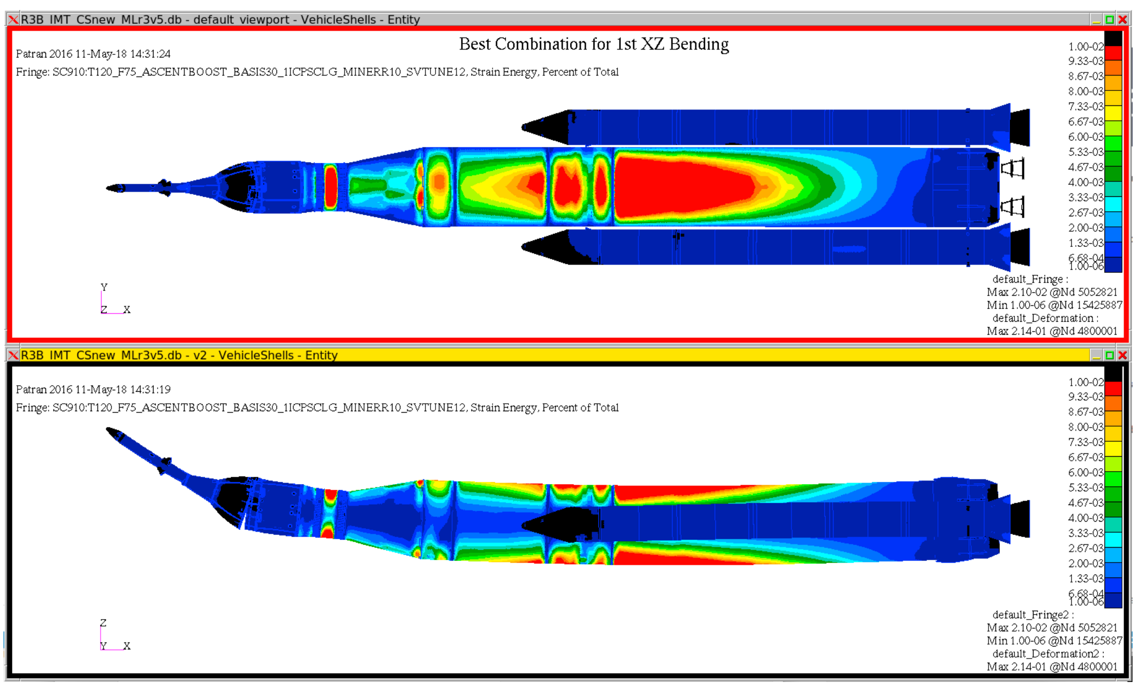

Figure 6. 1st XZ best combination of IMT modes on full model (ML not pictured).

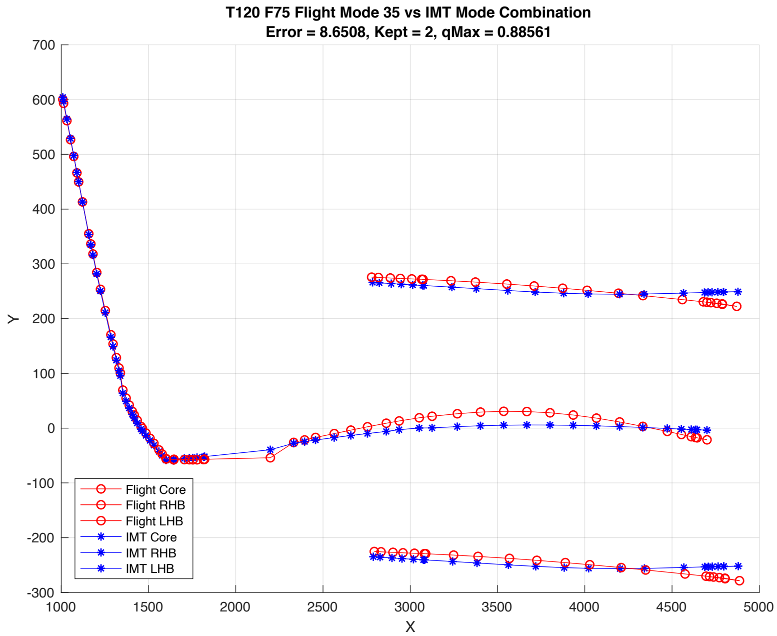

Figure 7. IMT vs. Flight Centerline deformations of 2nd XY bending mode

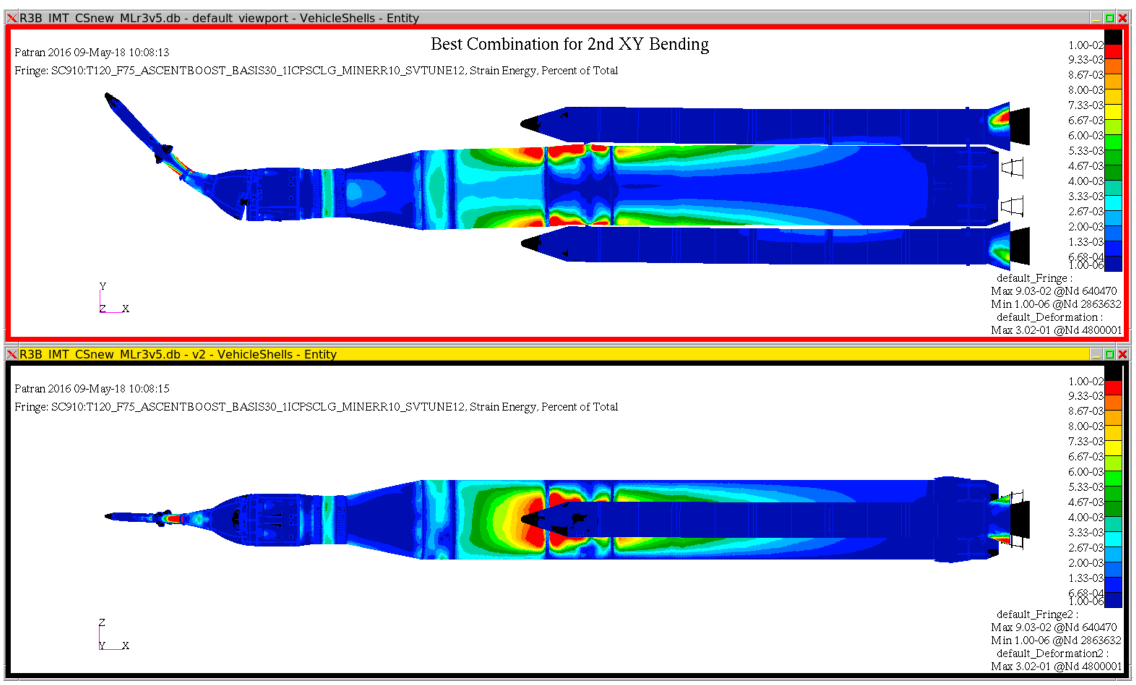

Figure 8. 2nd XY best combination of IMT modes on full model (ML not pictured).

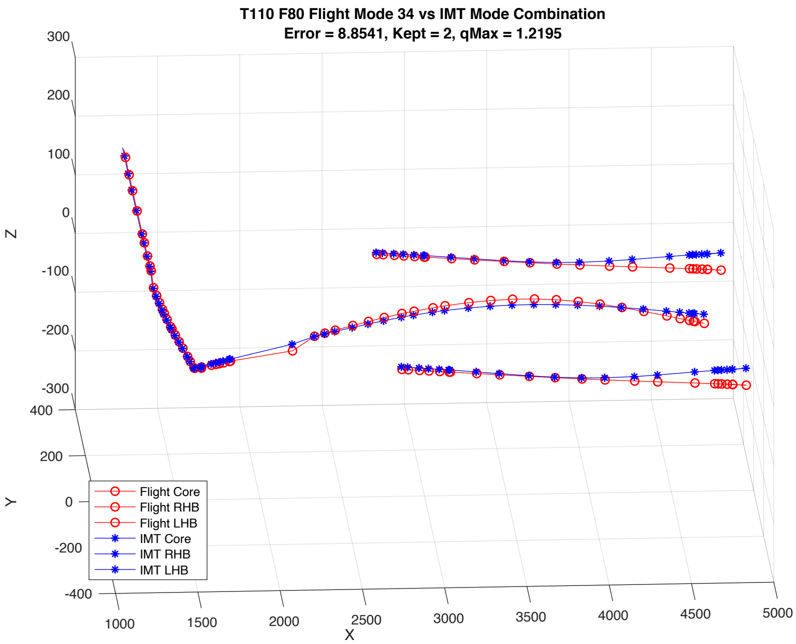

Figure 9. IMT vs. Flight Centerline deformations of 2nd XZ bending mode

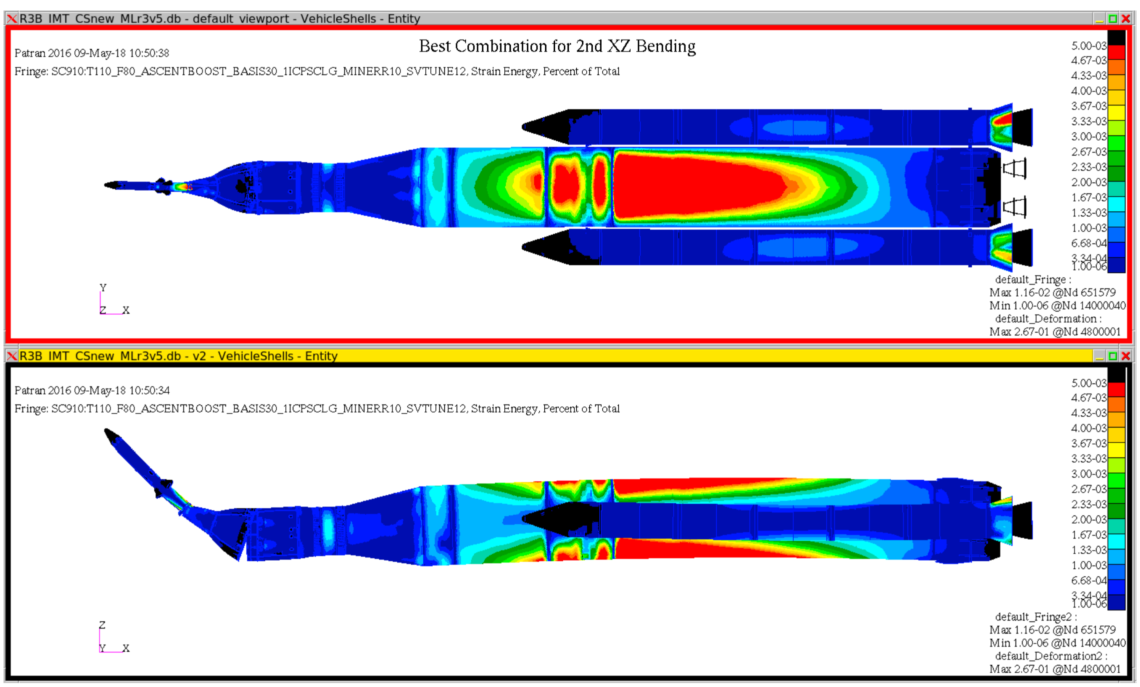

Figure 10. 2nd XZ best combination of IMT modes on full model (ML not pictured).

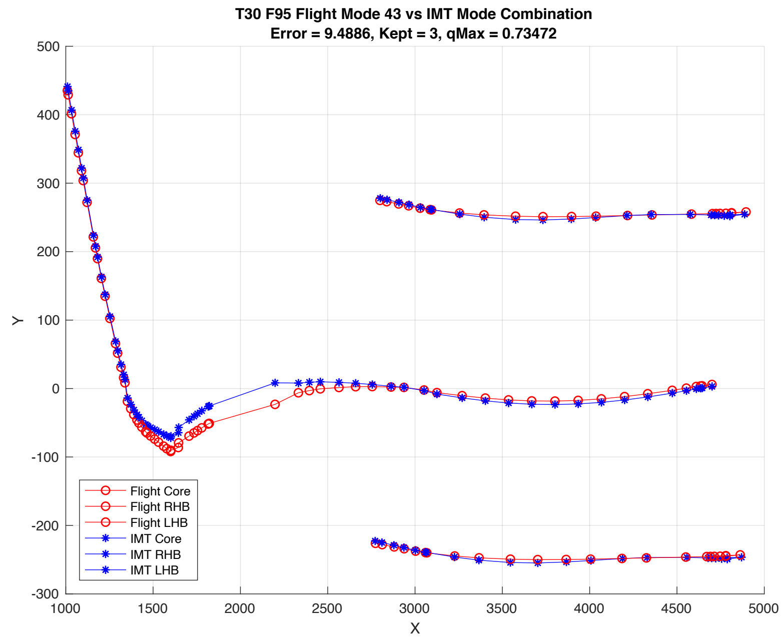

Figure 11. IMT vs. Flight Centerline deformations of 3rd XY bending mode

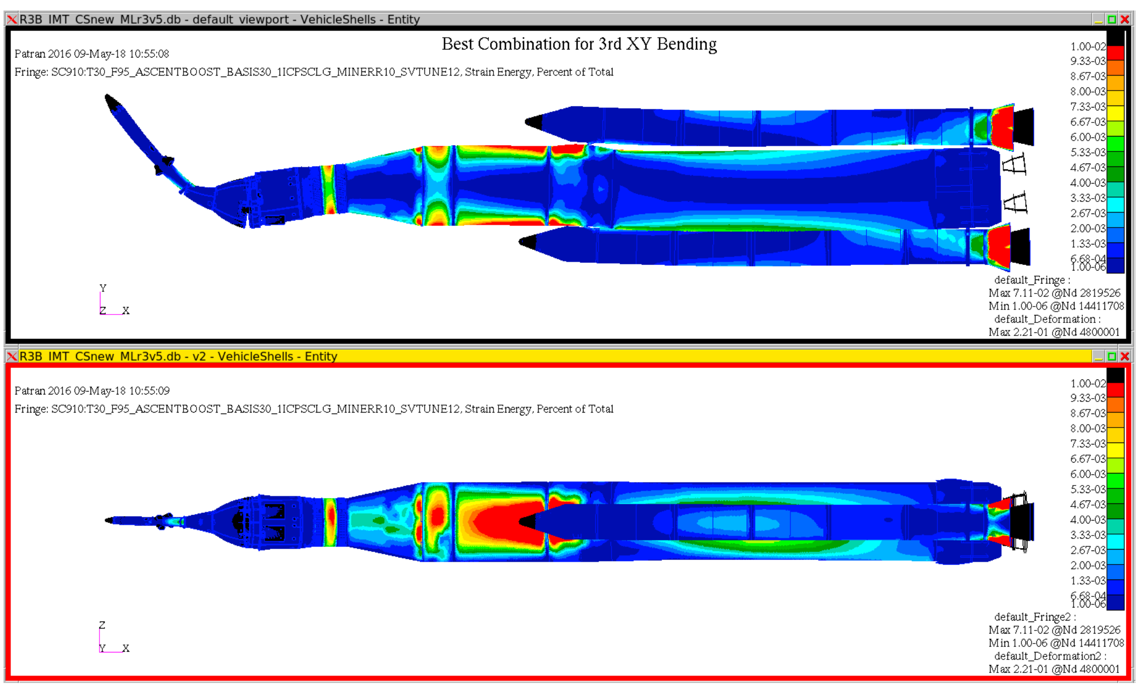

Figure 12. 3rd XY best combination of IMT modes on full model (ML not pictured).

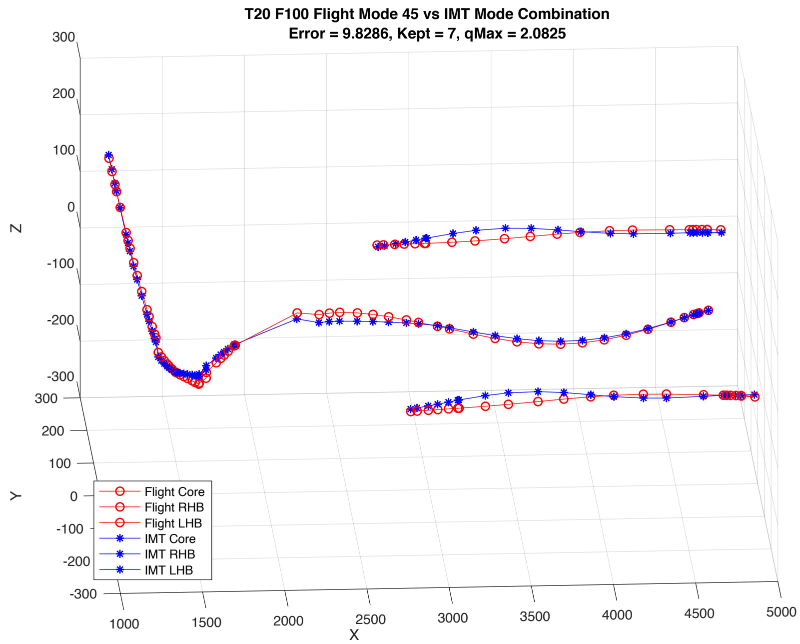

Figure 13. IMT vs. Flight Centerline deformations of 3rd XY bending mode

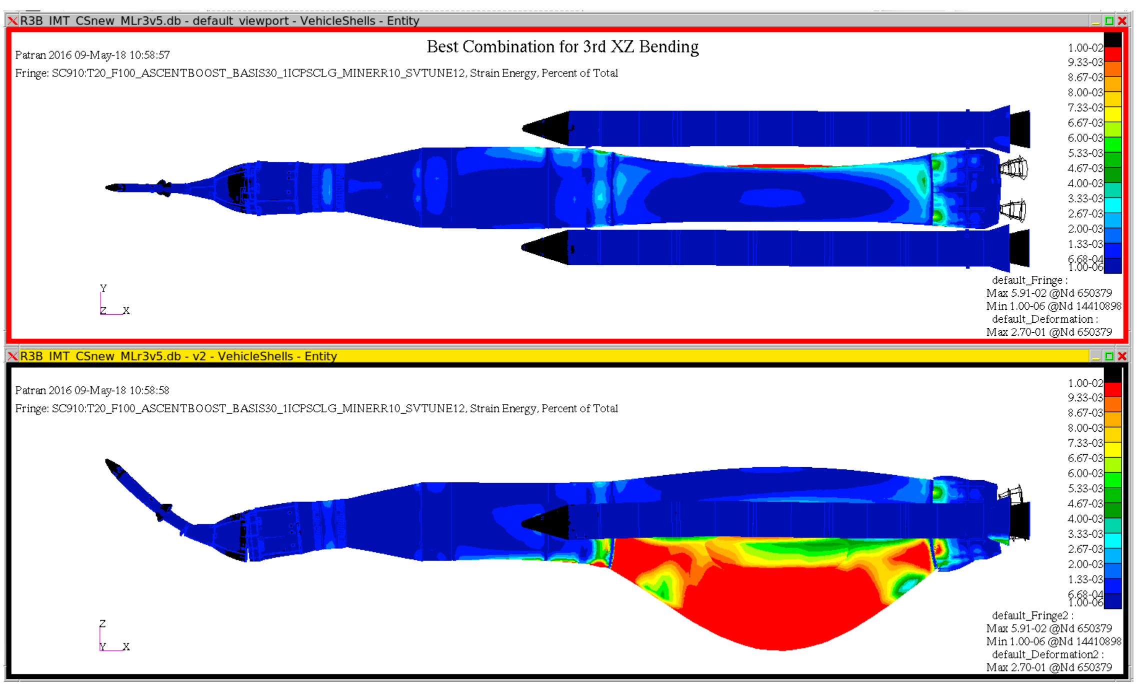

Figure 14. 3rd XZ best combination of IMT modes on full model (ML not pictured).

Figures 13 and 14 show a somewhat different message that what is seen in figures 3 through 12. If one had simply looked at Figure 13 it would be reasonable to conclude that another good match was found for the deformations in the core portion of the vehicle. However looking at Figure 14 it is seen that the LH2 portion of the core does not follow a simple 3rd XZ bending shape. Rather it shows a lot of shell deformation. This is one of the pitfalls of using centerline grids as the DOF to equate between flight and test and because the centerline grids are attached to the structure with NASTRAN RBE3 elements. In this situation it appears that the averaging of the independent DOF's used in the RBE3 element is mimicking the desired bending shape at the centerline. So the algorithm thinks it finds a good match to the global bending mode, when in fact it finds an asymmetric shell deformation.

It is possible that other grids could be used to equate which may avoid this problem, but unfortunately because the loads models are delivered as reduced models, there are not many physical grids to use for projection. And there are not any in the center of the LH2 tank, except for the centerline grids. While adding more physical grids or obtaining the displacements of alternate grids for projection is possible, the level of effort is beyond the scope of the present work.